A wavefront sensor-driven variable geometry pupil for ground-based aperture synthesis imaging

D.W. Tyler[a] and B.E. Stribling[b]

[a] University of New Mexico, Albuquerque High Performance Computing Center
1601 Central Ave. NE, Albuquerque NM 87131 USA

[b] Michigan Technological University, Dept. of Electrical Engineering
1400 Townsend Dr, Houghton MI 49931 USA

ABSTRACT

We describe a variable-geometry pupil (VGP) to increase image resolution for ground-based near-IR and optical imaging. In our scheme, a curvature-type wavefront sensor provides an estimate of the wavefront curvature to the controller of a high-resolution spatial light modulator (SLM) or micro-electromechanical (MEM) mirror, positioned at an image of the telescope pupil. This optical element, the VGP, passes or reflects the incident beam only where the wavefront phase is sufficiently smooth, *viz.*, where the curvature is sufficiently low. Using a computer simulation, we show the VGP can sharpen and smooth the long-exposure PSF and increase the OTF SNR for tilt-only and low-order AO systems, allowing higher resolution and more stable deconvolution with dimmer AO guidestars.

Keywords: Adaptive optics, Aperture synthesis, Optical instrumentation

1. INTRODUCTION

Time-varying, spatially random refractive index fluctuations in Earth's atmosphere limit the resolution of even the largest ground-based telescopes to that obtainable by a telescope of diameter equal to the Fried seeing parameter, r_o. This limitation can be understood by considering the effects of *pupil redundancy* in imaging while viewing image formation itself as an interferometric process.[1] In the interferometric model, the pupil of an Earth-based telescope is seen as an ensemble of r_o-size "apertures" or patches, each pair of which forms an interference pattern on the detector. The fringe patterns have a variety of orientations and modulation frequencies depending on the orientation and separation of these patches, and their incoherent sum is the detected image. In an unobscured telescope pupil in the presence of atmospheric turbulence, there may be many r_o patches separated by identical distances and having the same orientation. This means the fringe pattern in a given direction on the detector with a given frequency is actually the sum of many individual *redundant* fringe patterns. Due to turbulence, the phase difference between any two redundant fringe patterns is a random variable, reducing the visibility of the sum fringe pattern and limiting the resolution of the detected image. Use of adaptive optics (AO) increases resolution by reducing the relative shift of the individual fringe patterns and increasing the spatial coherence of the field incident at the telescope pupil, thus increasing the visibility of the sum pattern.[2] Another, less complicated approach is to limit redundancy by masking selected portions of the telescope pupil. Several relatively small openings can be used to synthesize a large, high-resolution telescope. While the phases of the resulting fringe patterns are still randomized by turbulence, the resulting increase in visibility *amplitude* SNR can be used to enhance phase recovery by such methods such as speckle imaging or self-calibration.[3] Of course, masking the light-gathering area of the telescope decreases the available signal and passes a reduced set of spatial frequencies. This technique is known variously as "optical aperture synthesis," "pupil" or "aperture masking," "non-redundant masking", and "masked-aperture speckle imaging." We use the nomenclature "partially-redundant masking" (PRM) as a general description of the several variations on the above theme.

Since the first astronomical images reconstructed using aperture masking[4] were reported in 1988, considerable effort has been expended by the astronomical community to quantify the viability of this technique,[5–10] especially in comparison with adaptive optics systems.[11] Initial studies and experiments were done using masks with a fixed (small) number of r_o-size openings. To obtain reasonable u-v coverage with a small number of apertures, researchers applied several rotations of the mask relative to the incident beam. More recently, workers employed more novel geometries, such as an r_o-size annulus[5,12] or a slit.[13] These geometries are not actually "non-redundant," hence the use of "PRM." Generally, AO is considered to be the more robust of the two methods, allowing deeper imaging at higher resolution. As a consequence, there has been some interest in combining the techniques.[14] In this paper, we describe an adaptive pupil mask for use with AO, driven by the AO wavefront sensor. As we will show, the concept has potential to augment the resolution provided by conventional AO.

The variable-geometry pupil (VGP) we propose here is a new type of adaptive optical element, correcting the amplitude of complex visibilities rather than the phase, and realizing PRM concepts in an adaptive, controllable way. Such an element might be a high-resolution spatial light modulator (SLM) or a micro-electromechanical (MEM) mirror. The VGP would be placed between the AO deformable mirror and the science instrument and controlled in such a way that only portions of the incident beam with sufficiently small phase variation would be passed (SLM) or reflected (MEM) to the science instrument. Since we envision the VGP would be used with AO, an estimate of the wavefront phase is readily available from the AO wavefront sensor (WFS). In fact, if the AO system uses a curvature-sensing WFS, the WFS provides the information on phase "smoothness" directly to the VGP controller. In our scheme, the WFS would drive the AO system in a closed control loop while providing "go-to" curvature signals to the VGP; that is, there would be no feedback between the VGP and the WFS. The VGP would thus receive commands at intervals on the order of the inverse AO bandwidth, passing or reflecting light in response to the random atmospheric phase perturbations and the AO system corrections. Since the phase of the wavefront incident at the WFS and VGP (modulo noncommon optical path errors) is a random process, the shape of the VGP would also change randomly, potentially providing full u-v coverage after a few WFS commands. The VGP, as we envision it, would overcome many of the limitations in the fixed-pupil PRM concept; for example, the VGP can be adjusted for seeing and object brightness conditions without modifying or replacing the mask, and there is no need for beam or mask rotation. We note that the concept of selectively masking the telescope pupil during AO operation is also discussed in Morossi, *et al.*[15] in these proceedings.

In the following section, we describe the computer simulation methods used to model the telescope, AO, and VGP. In Section 3, we present simulation results, showing PSFs and OTF SNR plots with and without the VGP for various AO systems. We summarize our work in Section 4.

2. COMPUTER SIMULATION AND MODELING

We model incoherent imaging with a 3.6-m telescope and two AO systems. The computer simulation we use generates independent random realizations of Kolmogorov turbulence. The AO subroutines actually model a Shack-Hartmann WFS rather than a curvature sensor, but we calculate curvature separately after generating the post-AO phase map. For the simulation results shown here, both the AO and VGP are driven by "go-to" commands in open loop.

After AO compensation, the wavefront curvature is calculated from

$$C(\mathbf{r}) \ = \ \mathcal{F}^{-1}\{\rho^2\Phi(\boldsymbol{\rho})\}, \tag{1}$$

where $C(\mathbf{r})$ is the curvature map at pupil coordinate $\mathbf{r}$, $\Phi(\boldsymbol{\rho})$ is the Fourier transform of the pupil phase map $\phi(\mathbf{r})$, and $\rho = |\boldsymbol{\rho}|$. Since the above operations are done on the same grid as the array representation of the $\phi(\mathbf{r})$, $C(\mathbf{r})$ varies on an unrealistically small scale. To model the finite sampling resolution of an actual curvature WFS, we calculate $\hat{C}$ from C by smoothing with a Gaussian filter having a FWHM corresponding to the subaperture size used in the sim. The VGP pupil function is formed by setting the telescope pupil function to zero wherever $\hat{C}$ exceeds a threshold value. A VGP pupil function, typical for the conditions described in the next section, is shown in Fig. 1. Subsequent to the calculation of the VGP pupil function, a generalized pupil function is formed by multiplying the phase screen and VGP pupil function. PSF images are formed from the squared modulus of the Fourier transformed generalized pupil function.

3. SIMULATION RESULTS

Our baseline imaging model consists of a 3.6-m telescope and a 37-actuator AO system. This configuration yields an actuator separation of 55 cm. The Shack-Hartmann WFS model has 30, 48-cm subapertures. In all our simulations, we use a WFS phase measurement standard deviation of 0.18 radians, corresponding to a guidestar magnitude of about 6 with a sampling rate of 1000 Hz. This small error means WFS noise is not the limiting factor in image resolution, although we choose seeing conditions of $r_o = 20$ cm at our imaging wavelength of 750 nm that are somewhat demanding for the AO system ($D/r_o = 18$). To avoid excessive WFS aliasing, we model wavefront sensing at H band, where the effective seeing parameter is ≈ 50 cm. The detector pixels are critically sampling, with each pixel subtending about 26 milli-arcsec. In these seeing conditions, the AO performance is partially-compensating due to fitting error, allowing for some resolution gain using the VGP, but not unrealistically degraded.

Fig. 1: Sample VGP pupil function. White indicates low-curvature regions. Note the telescope secondary obscuration is not readily apparent because it is contiguous with two regions of high wavefront curvature, which are masked by this realization of the VGP pupil function.

VGP operation is illustrated in Fig. 2. The top part shows a surface plot of the DM-only generalized pupil function. Notice the vertical scaling, indicating the wavefront phase, extends from -6 to +6 radians. While the DM-only AO has corrected much of the phase from the $D/r_o = 18$ seeing, the residual is significant. In the bottom of Fig. 2, we show a surface plot of the VGP/DM generalized pupil function. Note the scaling now extends from -4 to + 4, and regions with large phase excursions in the top part of Fig. 2 have been blocked by the VGP.

In Fig. 3, we show long-exposure log PSFs using the 30-subaperture AO system with and without the VGP. The PSFs were formed by averaging the images from 300 independent turbulence realizations. No detector noise is modeled for these plots, since we desire to see potential PSF improvements prior to noise modeling. To distinguish between the two types of AO, we refer to conventional adaptive optics without the VGP as "DM-only" AO. The use of both the DM and VGP is called "VGP/DM AO." Note the VGP/DM PSF has more energy in the diffraction-limited core and smaller halo features.

If we improve the DM correction by adding more subapertures and actuators, the improvement using the VGP is not so pronounced, as we expected. In Fig. 4, we show the same PSFs for AO with 40 subapertures and 45 actuators. Although the DM-only PSF has improved considerably, the VGP/DM PSF still has more core energy and smaller sidebands. Conversely, degrading the AO performance causes a dramatic increase in the relative performance of VGP/DM AO over DM-only AO. Fig. 5 shows PSFs for a 30-subaperture WFS driving a fast-steering mirror (FSM) for tilt removal and a VGP/FSM combination. In this case, the improvement in core energy using the VGP is nearly an order of magnitude; in fact, there is no discernible core without the VGP.

The implications of these improvements are illustrated in Fig. 6: Here, we have plotted the DM-only PSFs for the 30 and 40-subaperture systems along with the VGP PSF for the 30-subaperture system. Note the VGP PSF with the 30-subaperture AO has nearly the same core energy and lower sidelobes than the 40-subaperture DM-only PSF. Potentially, then, the VGP can extend the resolution obtained with DM-only AO to the dimmer guidestars allowed with fewer, larger subapertures.

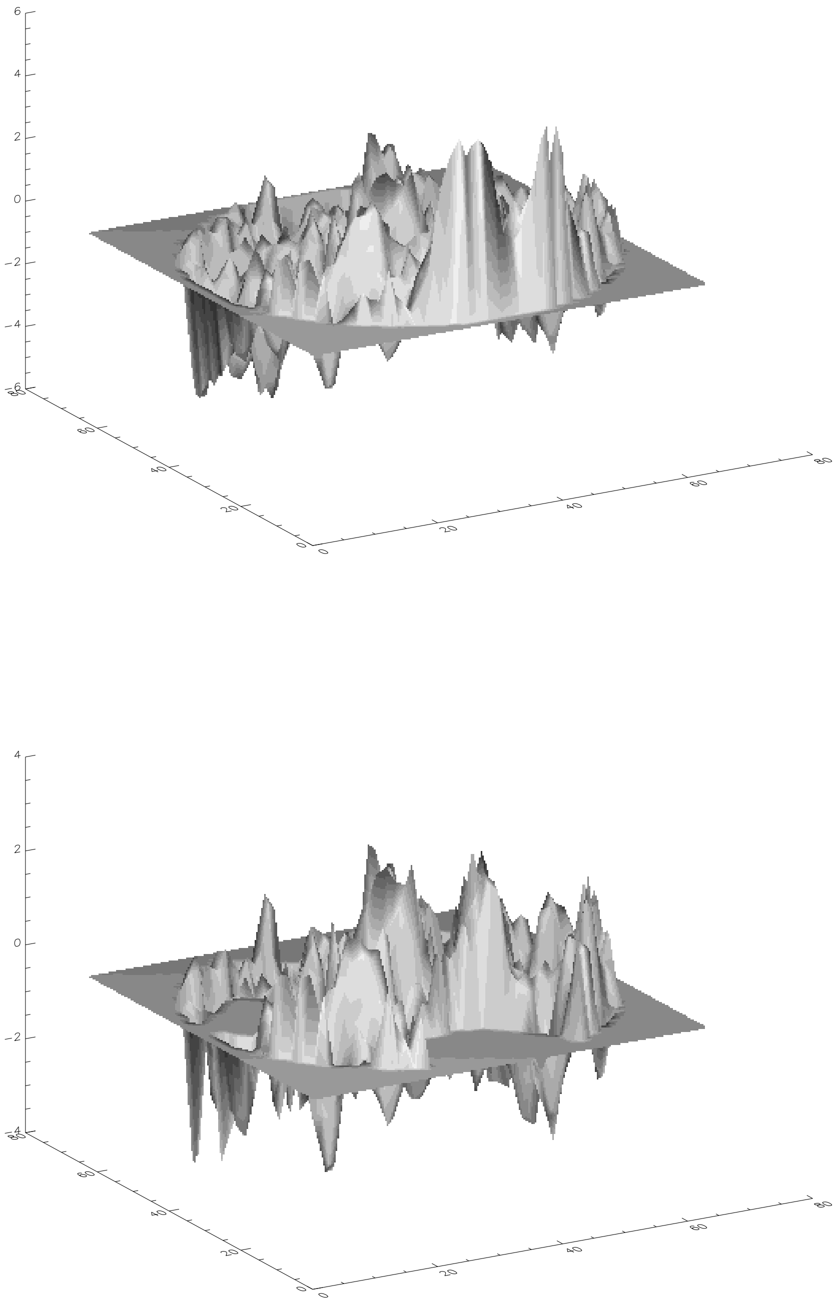

Fig. 2: DM-only (top) and VGP/DM (bottom) generalized pupil functions.

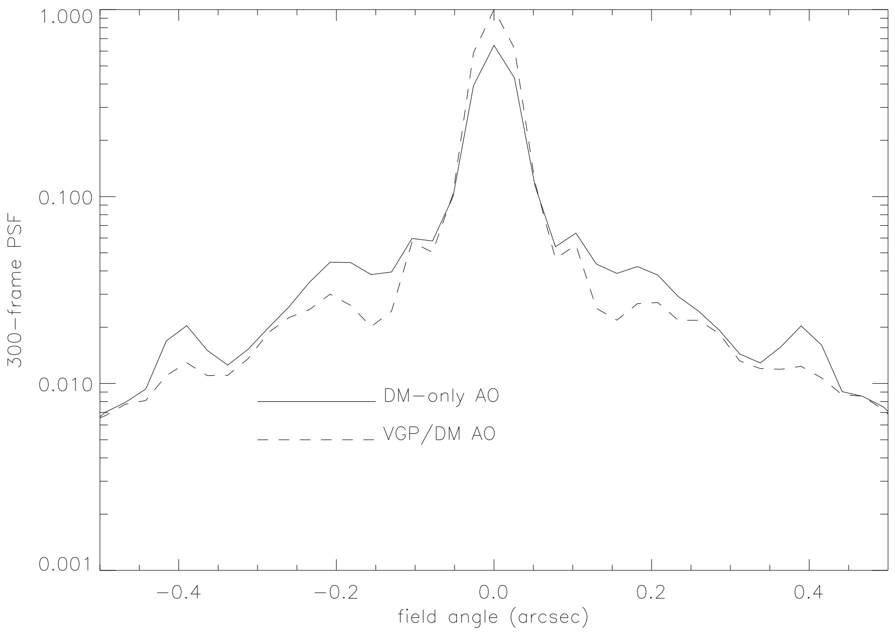

Fig. 3: Long-exposure log PSF cross-sections for a 30-subaperture WFS driving a 37-actuator DM only (solid line) and a VGP/DM combination (dashed line).

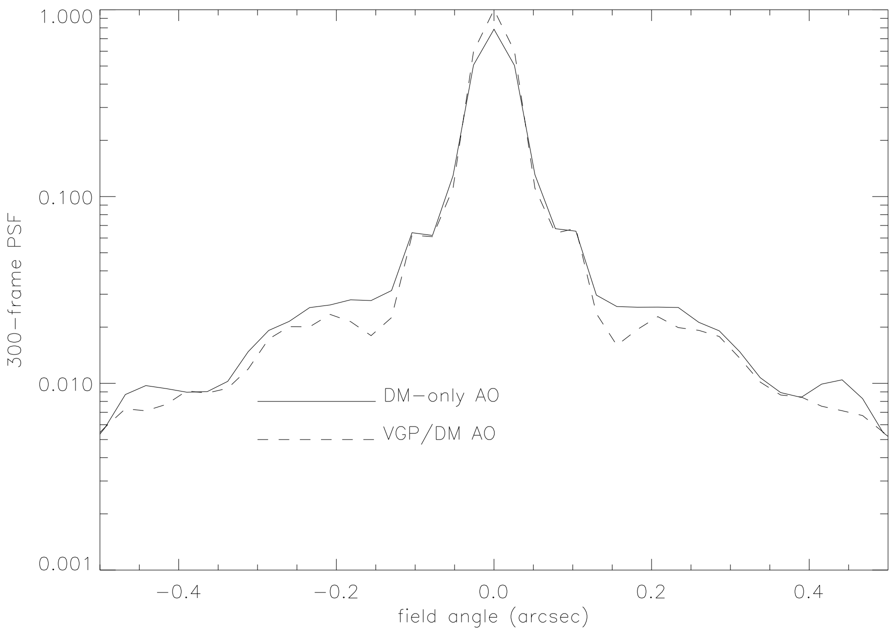

Fig. 4: Long-exposure log PSF cross-sections for a 40-subaperture WFS driving a 45-actuator DM only (solid line) and a VGP/DM combination (dashed line).

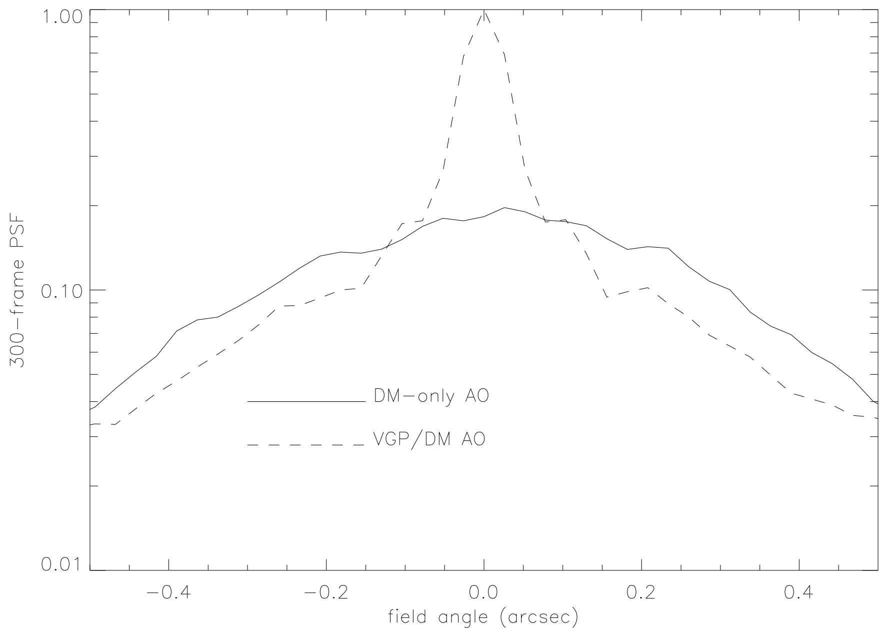

Fig. 5: Long-exposure log PSFs for a 30-subaperture WFS driving a tip-tilt FSM only (solid line) and a VGP/FSM combination (dashed line).

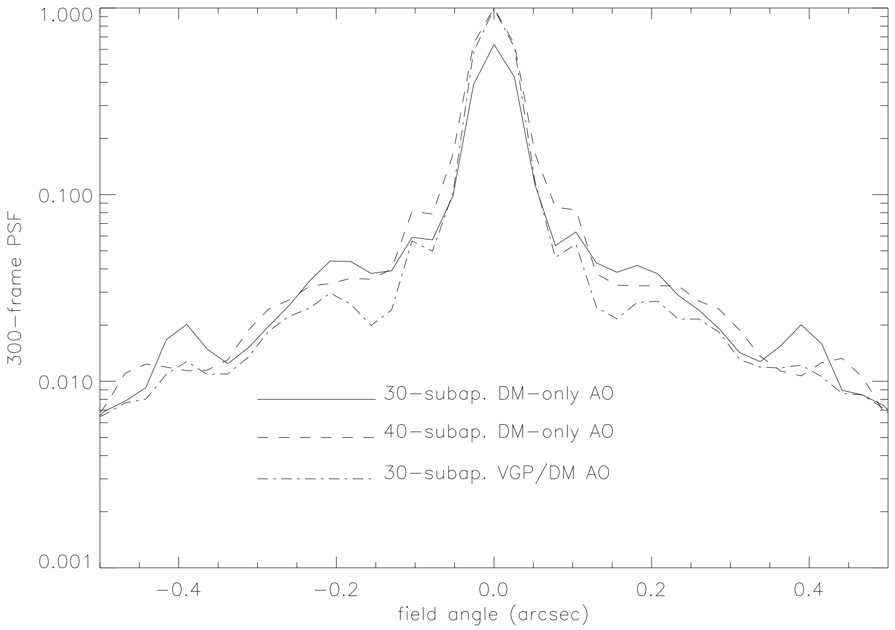

Fig. 6: Long-exposure log PSF cross-sections for a 30-subaperture WFS driving a 37-actuator DM only (solid line), a 40-subaperture WFS driving a 45-actuator DM only (dashed line), and a 30-subaperture WFS driving VGP/DM combination (dot-dashed line).

While improved PSF morphology is desirable, the key to successful deconvolution stability is the OTF SNR. To assess the relative SNR performance of VGP/DM and DM-only AO, we included detector noise in the image formation process and calculated sample SNRs over a 300-frame ensemble. For these simulations, we included Poisson (signal-dependent) noise from a double-precision random number generator and zero-mean Gaussian (additive) "read" noise with an RMS amplitude of 7 e^- per pixel per read.

In Fig. 7, we show the OTF SNR for a magnitude 10 object. The signal level to the WFS is unchanged, since we desire only to study the effect on the OTF SNR of reducing the signal level with the VGP. The 2-d SNR map has been radially averaged to produce a simpler x-y plot. Note the VGP/DM SNR is significantly higher than the DM-only SNR for all frequencies beyond the seeing spike. The relative reduction in VGP/DM SNR near DC is due to the increased fluctuation in total intensity as the VGP aperture area changes randomly; the only total count variance for DM-only AO is due to detector noise.

In Fig. 8, we show the same plots for a magnitude 12 object. The curvature threshold is the same as was used for all other plots shown here. Here, the DM-only SNR curve is slightly higher than the VGP/DM SNR at all frequencies of interest. Clearly, the SNR gains using the VGP are magnitude-dependent. However, we point out that with *fixed* aperture masks, there are two free parameters available to optimize measured visibility SNR[16]; namely, the size and number of the mask openings ("subapertures"). While there are not generally discrete subapertures in the VGP as there are with a fixed aperture mask, the ratio of turbulence noise power to detector noise power can still be manipulated by adjusting the wavefront curvature threshold and by restricting the regions over which the VGP can allow light to pass. For dim objects, larger subapertures are favored in fixed aperture masks, even though the turbulence power in the data increases. By analogy, dim objects should also drive a VGP controller to use a lower curvature threshold, increasing the pupil area. Dim objects also dictate a reduction in the number of fixed subapertures; this reduces the number of baselines among which light must be shared (naturally, this reduction in the number of subapertures becomes academic for objects so dim as to indicate aperture masking should not be used at all). The same effect can be obtained with the VGP by allowing the VGP controller to mask regions of the pupil regardless of the wavefront curvature. For example, the VGP could mask all but a small annulus of the pupil, only opening for low-curvature wavefronts within the area of the annulus. These ideas and optimal control rules will be studied in future work.

4. SUMMARY

We have described a variable-geometry pupil (VGP) to increase image resolution for ground-based near-IR and optical imaging. A curvature-type wavefront sensor provides an estimate of the wavefront curvature to the controller of a high-resolution spatial light modulator (SLM) or micro-electromechanical (MEM) mirror, which passes or reflects the incident beam only where the wavefront phase is sufficiently smooth, *viz.*, where the curvature is sufficiently low. Using a computer simulation, we have shown the VGP can sharpen and smooth the long-exposure PSF and increase the OTF SNR for tilt-only and low-order AO systems, allowing higher resolution and more stable deconvolution with dimmer AO guidestars.

We point out that the VGP can be used for long-exposure imaging, in contrast with fixed-aperture masks, which are typically used to enhance visibility SNRs in speckle imaging schemes. Also, we note that while the VGP/DM PSFs shown here have more core energy and smaller halo features close to the core, there is generally more energy in the VGP/DM halo at radii greater than about an arcsecond from the core. This is due to the fact that the VGP aperture area is bounded from above by the DM-only aperture area, and is most always smaller. Additionally, we note that where a curvature-sensing WFS is used, the VGP uses curvature information directly, rather than after integration, meaning the VGP controller is never subject to the numerical errors that can occur using a large number of subapertures in a curvature sensor. Finally, we point out that the sharper core obtained with the VGP could increase the sky coverage of an AO-compensated spectrometer[17] or the sensitivity of a coronographic imager.

ACKNOWLEDGMENTS

The authors gratefully acknowledge support from the USAF/MHPCC R&D Consortium. DWT acknowledges support from the Air Force Office of Scientific Research. When the work described in this publication was performed, DWT was employed at Schafer Corporation, Albuquerque, NM; he is personally grateful to Dr Rettig Benedict of Schafer and many others for his great experiences there. At the same time, BES was employed at the Air Maui Optical Station, AFRL/DEBI, Kihei, Maui, HI.

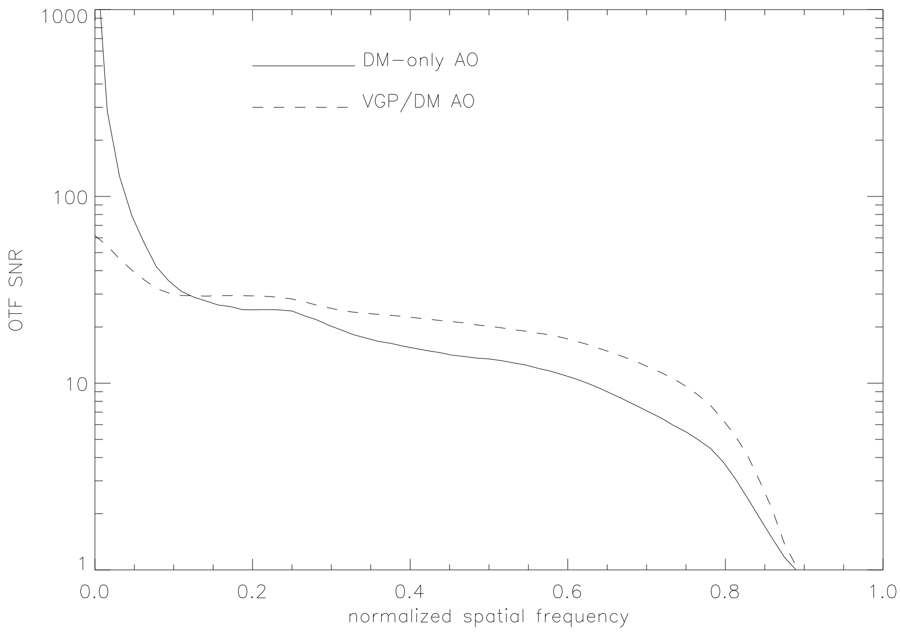

Fig. 7: OTF SNR curves for DM-only (solid line) and VGP/DM (dashed line) AO for a magnitude 10 object.

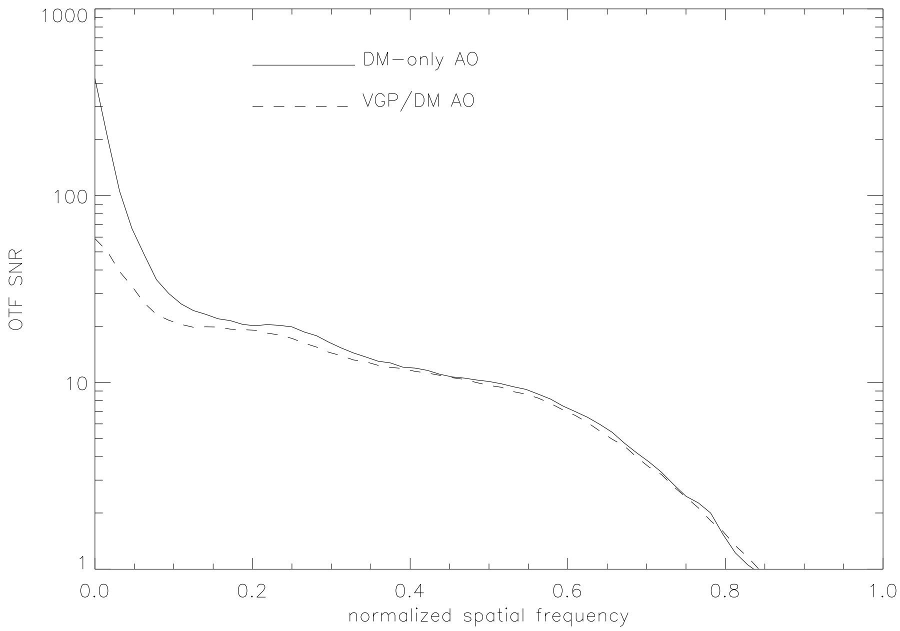

Fig. 7: OTF SNR curves for DM-only (solid line) and VGP/DM (dashed line) AO for a magnitude 12 object.

REFERENCES

1. J.W. Goodman, "Image Formation as an Interferometric Process", in *Statistical Optics*, p. 331, John Wiley and Sons, New York (1985)
2. M.C. Roggemann, *et al.*, "Compensated speckle imaging: theory and experimental results," Appl. Opt. **33**, p. 3099 (1994)
3. T.J. Cornwell, "Radio interferometric imaging of weak objects in conditions of poor phase stability: The relation between speckle masking and phase-closure methods", Astron. Astrophys. **180**, p. 269 (1987)
4. C. Haniff, *et al.*, "The first images from optical aperture synthesis", Nature (London) **328**, p. 694 (1988)
5. C.A. Haniff, D.F. Buscher, J.C. Christou, and S.T. Ridgway, "Synthetic aperture imaging at infrared wavelengths," Mon. Not. R. Astr. Soc. **241**, pp. 51p-56p (1989)
6. T. Nakajima, *et al.*, "Diffraction-limited imaging II: Optical aperture synthesis imaging of two binary stars", Astron. J. **97**, p. 1510 (1989)
7. J. Robertson, *et al.*, "High resolution imaging by optical aperture synthesis — first results from the MAPPIT project", Proc. Astron. Soc. **9**, p. 162 (1991)
8. W.N. Weir, *et al.*, "Infrared non-redundant mask imaging at Palomar", in *Amplitude and Intensity Spatial Interferometry*, J. Breckinridge, ed., Proc. SPIE **1237**, p. 274 (1990)
9. R.W. Wilson, J.E. Baldwin, D.F. Buscher, and P.J. Warner, "High-resolution imaging of Betelgeuse and Mira," Mon. Not. R. Astr. Soc. **257**, pp. 369-376 (1992)
10. C.A. Haniff, A.M. Ghez, P.W. Gorham, S.R. Kulkarni, K. Matthews, and G. Neugebauer, "Optical aperture synthetic images of the photosphere and molecular atmosphere of Mira," Astr. J. **103**, pp. 662-1667 (1992)
11. T. Nakajima and C.A. Haniff, "Partial adaptive compensation and passive interferometry with large ground-based telescopes", Pub. Astr. Soc. Pacific **105** (1993)
12. C. Haniff and D. Buscher, "Diffraction-limited imaging with partially redundant masks I: Infrared imaging of bright objects", J. Opt. Soc. Am. A **9**, pp. 203-218 (1992)
13. D. Buscher and C. Haniff, "Diffraction-limited imaging with partially redundant masks II: Optical imaging of faint sources", J. Opt. Soc. Am. A **10**, pp. 1882-1894 (1993)
14. C.A. Haniff and R.W. Wilson, "Closure-phase imaging with partial adaptive correction," Pub. Astr. Soc. Pacific **106**. pp. 1003-1014 (1994)
15. C. Morossi, M. Franchini, and S. Furlani, "Angular resolution improvement for an 8-meter class telescope via on-line subaperture selection," these proceedings.
16. D.W. Tyler, "Optimal pupil sampling for ground-based astronomical imaging I: Fixed-geometry pupils," *submitted* to JOSA-A.
17. D.W. Tyler and B.L. Ellerbroek, "Sky coverage calculations for spectrometer slit power coupling with adaptive optics compensation," in *Adaptive Optics Technologies*, Proc. SPIE 3353, D. Bonaccini and R.K. Tyson, *eds.*, pp. 201-209 (1998)